NASA Technical Memorandum 86408

RECENT TRANSONIC UNSTEADY PRESSURE MEASUREMENTS AT THE NASA LANGLEY RESEARCH CENTER

MAYNARD C. SANDFORD, RODNEY H. RICKETTS
AND ROBERT W. HESS

APRIL 1985

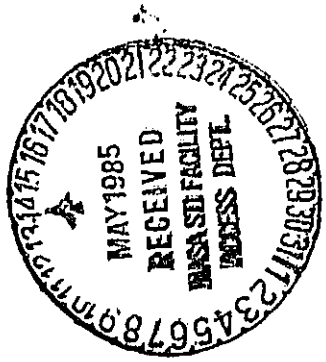

NASA
National Aeronautics and Space Administration
Langley Research Center
Hampton, Virginia 23665

Recent Transonic Unsteady Pressure Measurements at the NASA Langley Research Center

M. C. Sandford, R. H. Ricketts and R. W. Hess
NASA Langley Research Center
Hampton, VA 23665

Abstract

NASA Langley Research Center began an extensive program in the early nineteen seventies to measure unsteady pressures on lifting surfaces in transonic flow. Four semispan wing model configurations were studied in the Transonic Dynamics Tunnel (TDT). The first model had a clipped delta planform with a circular arc airfoil, the second model had a high-aspect-ratio planform with a supercritical airfoil, the third model had a rectangular planform with a supercritical airfoil and the fourth model had a high-aspect-ratio planform with a supercritical airfoil. To generate unsteady flow, the first and third models were equipped with pitch oscillation mechanisms and the first, second and fourth models were equipped with control surface oscillation mechanisms. The fourth model was similar in planform and airfoil shape to the second model, but it is the only one of the four models that has an elastic wing structure.

This paper describes the unsteady pressure studies of the four models and presents some typical results for each model. Comparison of selected experimental data with analytical results also are included.

Nomenclature

b	wing span, m
c	wing chord, m
C_L	total wing lift coefficient
C_p	pressure coefficient, $(p-p_\infty)/q$
f	wing pitch frequency, Hz
k	reduced frequency, $c\omega/2V$
M	freestream Mach number
p	local static pressure, kPa
p_∞	freestream static pressure, kPa
q	freestream dynamic pressure, kPa
R	Reynolds number based on wing average chord
t/c	thickness-to-chord ratio
V	freestream velocity, m/sec
x/c	fractional chord
α	pitch oscillation amplitude (peak), deg
α_o	mean angle of attack, deg
ΔC_p	lifting pressure coefficient (difference between lower and upper surface pressure coefficients)
$\lvert\Delta C_p\rvert$	magnitude of lifting pressure coefficient
δ	control surface oscillation amplitude (peak), deg
δ_o	mean control surface static angle, positive trailing edge down, deg
η	fraction of semi span
ω	circular frequency rad/sec

Introduction

The study of unsteady transonic flow is a vital and exciting field of research in aerodynamics. A fundamental understanding of the intricate physics of the problem is essential before we can fully cope with the highly nonlinear nature exhibited by transonic flow. The understanding of unsteady transonic aerodynamics is needed to incorporate the emerging structural, servoelastic, and aerodynamic technologies into the design of energy efficient transports, high performance and highly maneuverable fighter aircraft. There have been many accomplishments in unsteady transonic aerodynamics by researchers in the past decade as attested to in the excellent list of references of Edwards, Bland, and Seidel (ref. 1).

In the early nineteen seventies, NASA Langley Research Center began an extensive program to study experimentally unsteady transonic pressures on lifting surfaces. The purposes of these experimental studies were to obtain a large data base of pressure measurements that would assist in the design of advanced configurations and would help validate unsteady transonic aerodynamic analysis methods that are under development. Four large wing models have been tested under the current program and a photograph of each model is shown in Figure 1. The program began with two highly sophisticated semispan wing models. The first model was a highly swept, sharp-leading-edge, clipped delta planform configuration capable of being oscillated in pitch.[2] Two control surfaces, one leading-edge and one trailing-edge, could be oscillated independently. The second model was a moderately swept, rounded-leading-edge, high-aspect-ratio planform configuration equipped with multiple leading-edge and trailing-edge control surfaces that could be oscillated independently.[3] During the course of these studies, the need for a more basic wing model with a simple planform configuration became apparent. Therefore, the program was expanded to include an additional semispan wing model. This third model was an unswept, rounded-leading-edge, moderate-aspect-ratio, rectangular planform configuration capable of being oscillated in pitch.[4] All three of these models were made rigid as possible to minimize elastic deformations of the models. The program was expanded further with the selection of an elastic semispan wing model. This fourth model was very similar in airfoil shape and planform to the second model but had only a single trailing-edge control surface which could be oscillated.[5] Each of these four wing model configurations have been successfully tested in the Langley Transonic Dynamics Tunnel (TDT). Both steady and unsteady pressure measurements have been made along with some loads data, such as bending moments and control surface hinge moments, and tip deflections and twist for the elastic wing.

This paper describes the four unsteady pressure studies accomplished to date. The physical properties of the four models are described and some experimental techniques applied

to both model fabrication and unsteady pressure measurements are discussed. Typical results from each of the four tests are presented along with correlation of selected experimental data with analytical results. In addition, a few observations are made about future wind-tunnel pressure studies at NASA Langley.

FIRST MODEL - CLIPPED DELTA PLANFORM

Wind-Tunnel Model

Wing

The pertinent configuration parameters of the wing are given in the sketch in Figure 2. The clipped delta, semi-span, wing had a sweep angle of 50.45 degrees, an aspect ratio of 2.48, and a circular arc airfoil with a 6-percent thickness ratio. The semispan was 1.143 meters and the root chord was 1.614 meters. The pitch axis was located at 65.22 percent of the root chord. At the first wing resonant frequency, 28 Hz, there were significant dynamic bending deflections outboard of the control surface which restricted the maximum excitation frequency to 22 Hz.

The wing was constructed of stainless steel ribs and spars with a Kevlar-epoxy skin and weighed 53.933 kgm. The trailing edge control surface was a graphite epoxy structure built around a step-tapered steel shaft. For the test reported herein, a dummy leading edge control was substituted for the movable control.

Wing Mounting and Oscillation System

The wing was mounted on a hydraulically driven oscillating drive system on the sidewall of the Langley TDT as shown in Figure 3. The wing was supported on a tapered shaft which was oscillated in pitch by a hydraulic system as shown in Figure 4. A splitter plate was used to avoid the undesirable tunnel wall boundary layer flow. A wing fence at the root of the wing was designed to seal the wing at the juncture with the splitter plate. The wing static position and the dynamic amplitude were controlled by an electro-mechanical system and a hydraulic system, respectively. The dynamic system was designed to be operated as a spring-mass system at a resonance condition in pitching using heavy tuned springs (see Figure 4). Previous experience with driven airfoils had indicated that a spring-mass system would be desirable in that it would result in a lighter loading on the drive mechanism. In practice the springs were tuned to only one stiffness and the mechanism was operated at off-resonant frequencies, since it would have been necessary to enter the tunnel to change the effective stiffness. It was also necessary to preload the springs to one degree deflection to eliminate load reversal in the system through the range of oscillation amplitude. A separate hydraulic system drove the control surface position, both static and dynamic. Each hydraulic system was controlled by servo feedback systems.

Instrumentation

The wing was instrumented with 76 dynamic pressure transducers and 81 steady pressure orifices. The location of the upper surface transducers and static orifices are shown in Figure 2. There were nine accelerometers mounted in the wing to measure the dynamic amplitude including the effects of deflection due to chordwise bending. The control surface deflection and the model mean angle of attack were measured with potentiometers. The wing oscillation amplitude was measured with a linear variable differential transformer. Strain gage bridges on the wing structure and in the control surface shaft measured strain and moments for loads monitoring purposes.

Data Acquisition and Analysis

Test Conditions

The wing was tested in the Langley Transonic Dynamics Tunnel (TDT) in Freon* at $M = 0.90$, $q = 9.34$ kPa and at a Reynold's number of approximately 10 million based on the mean chord length of 0.921 m. Boundary layer transition strips were fixed on the upper and lower wing surface at 8 percent of local chord from the leading edge. The grit size varied from number 70 at the root to number 90 at the tip.

Data Reduction

The static and dynamic data were recorded digitally at the rate of approximately 950 samples per second per channel. Data acquisition and display were under control of the facility computer.[6] The upper surface steady pressure measurements were converted to engineering units and analyzed during the test. However, the dynamic data were analyzed post-test to determine the Fourier coefficients from which the magnitude and phase were determined.

Since this was a symmetric airfoil, all the transducers were located on the upper surface. The upper surface pressures were measured at a positive angle of attack and the lower surface pressures were obtained from the upper surface pressures measured at a negative angle of attack. The lifting pressure distribution ΔC_p, steady and unsteady, was computed from the difference of the upper and lower corresponding sets of data.

Steady Calculations

Steady pressure distributions for pitch and control surface deflections were computed using the modified three-dimensional, transonic small disturbance, Bailey-Ballhaus code.[7] This code has options for modeling a viscous boundary layer. However, the inviscid option, used in the present paper, gave the best comparison with measured data in that the experimental shock location is further aft.

*Freon is a registered trademark of E.I. DuPont de Nemours & Co., Inc. Use of trade names does not constitute an official endorsement, either expressed or implied, by NASA.

Results and Discussion

Steady Pressure Results

The experimental and calculated chordwise pressure distributions of ΔC_p are shown in Figures 5 and 6 for pitch and control surface deflection, respectively.

The variation of steady lifting pressure with angle of attack is shown in Figure 5 for the three spanwise locations. The symbols represent the experimental results and the lines represent the analytical results. Agreement between the experimental and analytical results is good for the lower values of α_0 but deteriorates above α_0 = 2 degrees at the outboard stations. The theory is not equipped to handle what is believed to be vortex flow generated by the sharp leading edge. This vortex expands toward the outboard stations as α_0 is increased.

The variation of static lifting surface pressure with control surface angle is shown in Figure 6 for three spanwise locations. The symbols represent the experimental results and the lines represent the analytical results.

The agreement between experiment and analysis is reasonable for small values of $\delta_0 = \pm 2$ degrees. However, at large deflection, $\delta_0 = \pm 6$ deg, the analysis predicts more negative and larger ΔC_p pressures, near the hinge line at x/c = 0.80, than were measured. The agreement between the experimental and analytical results for variation in α_0 and δ_0 is best at the inboard stations.

Unsteady Pressure Results

Wing Pitch Oscillations.- The pressure magnitude and phase angle results for wing pitch oscillation of 0.5 degrees for angles of attack of 2 and 4 degrees at η = .70 are given in Figure 7. A peak in the magnitude is evident near the hinge line of 80 percent of chord and increases as frequency increases. Due to the location of this peak, it apparently is caused by the motion of the mean shock. An abrupt change in phase angle occurs at this peak in $|\Delta C_p|$. Another more dominant peak appears in the α_0 = 4 degree data near the leading edge which is less affected by frequency. Due to the location of this dominant peak, it probably is caused by the motion of the leading edge vortex flow. No significant change in phase angle occurs at this dominant magnitude peak. The phase distribution for the 4 degree data differs from the α_0 = 2 degrees data in that the phase is negative at the leading edge in the region of the flow separation.

Control surface oscillations.- Figure 8 shows unsteady pressure magnitude and phase angle results due to control surface oscillation for several values of amplitude, δ, and frequency, f, for static wing angles of attack, α_0, of 2 and 4 degrees. A large peak in the magnitude is evident near the control surface hinge line. This large peak probably is caused by both the control surface motion and the mean shock motion. There are no pronounced effects on the magnitude of the lifting pressure, $|\Delta C_p|$, due to control surface oscillation frequency. There is a distinct difference in the phase angle for the two frequencies of Figure 8. The phase angle is the same aft of the control surface hinge line.

Concluding Remarks For The First Model

Some static and oscillatory pressure results are given for a small range of parameters at 0.9 Mach number for a clipped delta wing with a circular arc airfoil.

Calculated steady pressure results from the Bailey-Ballhaus code compared well with the static experimental data for wing angles of attack or control surface deflections less than 2 degrees. At higher angles of attack, vortex flow from the sharp leading edge is believed to preclude satisfactory comparison, since nonlinear conditions for such flow are not accounted for in transonic small disturbance theory.

The dominant features of the oscillatory wing pitch results are the changes in the pressure magnitude induced by the motion of the mean shock, and the motion of the leading-edge vortex flow at α_0 = 4 degrees. The phase shift due to leading edge vortex flow was insignificant.

The effects of oscillatory control surface frequency on the magnitude of the lifting pressure were small. A distinct phase shift occurs forward of the hinge line due to change in frequency of the control surface motion.

SECOND MODEL - HIGH ASPECT RATIO PLANFORM

Wind Tunnel Model

General

The model consisted of a half-body fuselage similar to that of a "wide-body" transport and a rigid semispan wing representative of current energy efficient transport designs. The model was mounted on the tunnel sidewall to a turntable mechanism which allowed the mean angle of attack to be varied (see Fig. 9).

Geometry

A sketch of the wing is presented in Fig. 10. The wing had a leading-edge sweepback angle of 28.8 deg, an aspect-ratio of 10.76, and a semispan of 2.286 m. The side of the half-body fuselage was located at a wing station 0.219 m.

The wing was equipped with 10 oscillating control surfaces. Figure 10 shows five leading-edge control surfaces hinged about the 15% chord and five trailing-edge control surfaces hinged about the 80% chord. For the wind-tunnel tests presented herein only two trailing-edge control surfaces, shown in Fig. 10 by the cross- hatched areas, were oscillated to generate unsteady airloads. These two control surfaces are designated hereafter as the inboard control surface and the outboard control surface.

The wing contour was formed from three different supercritical airfoils. These three air-

foils were located at wing stations 0.219, 0.876, and 2.286 m and had thickness-to-chord ratios of 0.16, 0.14, and 0.12, respectively. The three supercritical airfoil shapes are shown in Fig. 11. Straight line interpolation along constant percent chords was used between adjacent airfoil sections. The section twist angles at each station, referenced to a horizontal reference plane, also are shown in Fig. 11.

Construction

The wing was constructed from aluminum alloy and consisted of upper and lower sections. Each section was stiffened in bending by a boron filament insert bonded to the internal cutout area shown in Fig. 12. The sections were permanently bonded together to form a box cross section. This type of construction produced a stiff, lightweight wing structure whose fundamental frequency (23 Hz) was well above the maximum control surface excitation frequency of 15 Hz used during the tests. These requirements for a stiff, high-frequency wing structure were dictated by the need to minimize the dynamic and static deformations of the model due to aerodynamic loads[8].

Lightweight control surfaces were constructed using stiff Kevlar-balsawood sandwich material thereby minimizing the control surface inertia loads and deformations. A typical control surface and actuator is shown in Fig. 13. Miniature hydraulic actuators[9] of the rotating vane type were used both to position the control surfaces statically and to oscillate them at deflection angles of ±6 deg over a frequency range from 5 to 15 Hz.

Instrumentation

The model was instrumented with 252 static pressure orifices and 164 in situ dynamic pressure transducers. Small precision potentiometers were used to measure directly the control surface angular displacement. The model root angle of attack was measured by a digital encoder that was attached to the turntable in the wind-tunnel wall. The wing was mounted to a five-component balance which measured the wing static forces and moments. Six accelerometers were installed in the model to detect wing vibrations.

Data Acquisition and Analysis

General

Acquisition of data from the large number of varied sensors located on this model and analysis of these data in a "near real-time" manner required the use of a computer. The TDT facility has a computer uniquely designed and programmed for this purpose.[6] The following paragraphs describe the data acquisition and analysis procedures used during the tests.

Steady Pressure Data

Steady pressures were measured using six 48-port scanning valves that were stepped simultaneously from port to port. For each measurement, the pressure was allowed to settle for 0.3 second and then was averaged for approximately 1 second to acquire a mean value of pressure coefficient for each orifice.

Unsteady Pressure Data

Pressure time-history signals from the transducers were digitized and recorded on magnetic tapes for 75-100 cycles of control surface oscillation. During playback of the digital tapes, the Fourier components of the data were determined at the frequency of oscillation of the control surface. Values of pressure coefficient magnitude and phase angle relative to the oscillating control surface position were calculated for each transducer.

Results and Discussion

General

Data from those tests included both steady and unsteady pressure measurements[10,11,12]. Although force-balance results are not presented herein, the drag rise characteristics, along with the steady pressure distributions do exhibit characteristics expected of supercritical wing aerodynamics[13]. The following discussions focus on the steady and unsteady pressure results for the design condition: $M = 0.78$, and $\alpha = 2.05$ deg. The Reynolds number was 2.2×10^6 based on the average wing chord. Comparisons between measured and calculated results are presented for chordwise distributions of unsteady lifting pressures.

Measured Steady Results

Chordwise pressure distributions of the upper and lower surfaces are shown in Figure 14 for several mean angles of attack. These results are for $\eta = 0.19$ and $\eta = 0.71$ at $M = 0.78$. The upper surface data show that for $\eta = 0.71$ a shock occurs at approximately 40 percent of chord for 2° angle of attack.

Lifting pressure distributions are shown in Figure 15 for several static control surface deflections for $M = 0.78$ and $\alpha_0 = 2.05°$. These chordwise pressure distributions are shown for two span locations ($\eta = 0.19$ and 0.71) which are near the midspan of the inboard and outboard control surfaces. The inboard results are reasonably smooth and linear for δ values between 6° and -6°, whereas the outboard results are not as smooth and show nonlinear characteristics.

Measured Unsteady Results

Inboard Control Surface Deflection and Frequency Results.- Chordwise distributions of lifting pressures due to oscillations of the inboard control surface at 10 Hz are shown in Fig. 16 for span stations $\eta = 0.19$ and $\eta = 0.71$. Results are given for oscillatory deflection angles δ of 2, 4, and 6 deg. First, observe the results for $\eta = 0.19$ which is near the midspan of the inboard control surface. The lifting pressure magnitude increases rapidly from a small value at the leading-edge $x/c = 0$ to a peak near the 80% chord (control surface hinge line) and then decreases very rapidly to a small value near the trailing-edge $x/c = 1.0$. The corresponding phase angle results show a large

phase lag near the leading edge that decreases to zero near the 65% chord and shows a phase lead over the rear portion of the chord. The magnitude of ΔC_p increases with control surface deflection amplitude in an approximate linear manner over the entire chord. That is, the magnitude of ΔC_p for δ = +6 deg is about three times the value for δ = +2 deg. The phase angle results essentially are independent of the amplitude of control surface deflection.

Second, observe the results of η = 0.71 which is near the midspan of the outboard control surface. Although the oscillating control surface is well removed from the pressure measurement station, its effect on the unsteady pressures is significant. The magnitude rises sharply to a peak near the 25% chord, drops abruptly to near zero at the 40% chord and remains near zero to the trailing edge. Except for the wide excursions in phase angle near the 40% chord, the phase angle trends for the outboard station are similar to those at the inboard station in that a large phase lag exists at the leading edge and decreases toward zero going rearward along the chord.

The chordwise distributions of lifting pressures for three frequencies of the inboard control surface oscillating at amplitude of 6 deg are presented in Fig. 17 for η = 0.19 and η = 0.71. Results are shown for frequencies of 5, 10, and 15 Hz which correspond to reduced frequencies k of about 0.1, 0.2, and 0.3. For η = 0.19, control surface frequency has a much greater effect on phase angles than on magnitudes of unsteady pressures. The largest effects occur at the leading edge where the 5 Hz data show a phase lag of about 120 deg. For η = 0.71, the results indicate the effects of frequency to be much more pronounced in the phase angle data than in the magnitude data. These results show again the significant influence the inboard oscillating control surface has on unsteady lifting pressures far outboard on the wing.

Outboard Control Surface Deflection and Frequency Results.- Unsteady lifting pressure distributions for the oscillating outboard control surface are presented in Figs. 18 and 19. The deflection amplitudes and frequency effects show general trends similar to those discussed for the oscillating inboard control surface. A significant difference, however, is the sharp hump in the lifting pressure magnitude data near the 50% chord. Although data for η = 0.19 are not presented in the figures, neither the magnitude nor phase angle data at this station was affected by the oscillating outboard control surface.

Comparison of Measured and Calculated Results

General.- The calculated results presented herein were obtained from an analysis based on linear theory for the acceleration potential on zero thickness lifting surfaces.[14] This subsonic kernel-function method accounts for edge and hinge line singularities of the control surface. Effects of airfoil thickness are partially accounted for by modifying the local streamwise velocity. Though not presented herein, more extensive comparisons with the experimental results using doublet lattice calculations are presented in ref. 15.

Chordwise Lifting Pressure.- A comparison between measured and calculated chordwise distribution of lifting pressures at η = 0.19 generated by oscillating the inboard control surface is presented in Fig. 20. These results are for M = 0.78 and control surface frequency of 10 Hz. The variation of lifting pressure magnitude per degree and of phase angle, referenced to the control surface position, is plotted as a function of fraction of chord. Measured and calculated magnitude results show reasonable agreement up to the 20% chord. From 20 to 70% chord, the calculations underestimate the measured data which are characterized by a broad hump that peaks near the 50% chord. Calculations overestimate measured data behind the hinge line at 80% chord. The calculated results show a smaller phase lag than the measured data ahead of the 40% chord. Aft of the 40% chord, the calculated and measured phase results are in good agreement.

Concluding Remarks For the Second Model

An experimental investigation has been conducted on an aspect ratio 10.8 supercritical wing model with oscillating control surfaces. Selected measured steady and unsteady results from the wind-tunnel tests have been presented and discussed. Briefly, the measured results show that unsteady lifting pressures generated by oscillating control surfaces are substantial. In particular, the inboard oscillating control surface was shown to have a significant influence on the unsteady lifting pressures far outboard on the wing. Also, measured data were compared with calculated results obtained using a subsonic lifting surface theory. Results indicate a need for prediction methods in the transonic speed range that are better than the RHOIV analysis in this study.

THIRD MODEL - RECTANGULAR PLANFORM

Wing Configuration

A photograph of the wing installed in the TDT is shown in Fig. 21. The wing is attached to a shaft that extends through a splitter plate mounted off the wind-tunnel wall so that the wing root is outside the wall boundary layer. The shaft is connected directly to a hydraulic rotary actuator that oscillates the wing in pitch.

The planform and airfoil shape are shown in Fig. 22. The unswept wing has a rectangular planform with a 0.61m chord and a 1.22m span (panel aspect ratio of 2.0). The airfoil is a 12% thick (t/c = 0.12) supercritical shape with a two-dimensional design Mach number of 0.8 and design lift coefficient of 0.6. This airfoil was chosen as being typical of those being employed on new transport aircraft. The wing tip was formed by connecting the upper and lower surfaces with semicircular arcs. The wing pitch axis is located at the 0.46 fractional chord. Details of the geometric properties, including

the airfoil coordinates, and the structural properties of the wing are presented in Ref. 16.

Instrumentation

Wing instrumentation consisted of 126 differential pressure transducers, eight accelerometers, and one potentiometer. The transducers were mounted at four spanwise stations to measure both steady and unsteady dynamic pressures along chordwise rows (see Fig. 22) on the upper and lower surfaces. Both in situ transducers and transducers utilizing the matched-tubing technique developed by Tijdeman[17] were mounted in the wing. Each transducer was referenced to the freestream static pressure. The potentiometer and accelerometers were used to measure static and dynamic motions of the wing. Details of the instrumentation are presented in Ref. 16.

Data Acquisition and Reduction

Data from the model instrumentation were acquired using the TDT real-time data acquisition system.[6] Steady pressures were measured using the differential pressure transducers installed in the wing. One thousand samples of data at a rate of 300 samples per second were averaged for each transducer to determine mean values of pressure coefficient. Unsteady pressures were calculated from transducer time-history data measured at a rate of 300 samples per second and recorded on digital tape. A discrete Fourier transform of 75-100 cycles of the data (a minimum of 15 samples/cycle) was used to determine the first harmonic pressure coefficient magnitude and phase in relation to the pitch position of the wing root. The magnitude and phase measurements from transducers using the matched-tubing method were determined using transfer functions derived from calibration data of corresponding in situ and matched-tubing transducers.

Test Results and Discussion

As illustrated in Fig. 23, steady and unsteady pressures were measured[18] for a large number of test conditions in the TDT. The figure shows the wing total lift coefficient plotted against Mach number for angles of attack ranging from -1 to 7 deg. For the unsteady-data points (solid symbols) in Fig. 23, the wing oscillation frequencies were 5, 10, 15, and 20 Hz. Some representative results obtained during these tests are presented. The Reynolds number based on the chord length is four million for all data presented.

Steady Results

Upper- and lower-surface steady pressure distributions at the four spanwise stations are shown in Fig. 24 for a Mach number of 0.825 and an angle of attack of 4 deg. (This is close to the two-dimensional design condition for the airfoil.) At the inboard sections (η = 0.31 and 0.59), typical supercritical flow is present on the upper surface, that is, there is a rather flat pressure region followed by a weak shock far aft (0.50 to 0.60 fractional chord) on the wing. However, for sections farther out on the wing, this shock is farther forward toward the leading edge as a result of the wing tip effects. Near the wing tip the shock is located at about the 0.10 fractional chord. The pressure distributions on the lower surface are not significantly affected by the presence of the wing tip.

Unsteady Results

Some of the unsteady pressure distributions measured during the tests are summarized in this section. The results are presented in terms of the magnitude and phase angle of the lifting pressure coefficient. In the Figures (25, 26, 27) presented in this section, curves are faired through the data points in the region of the shock to show trends and estimated peak-pressure (shock) locations.

Span Effects

Pressure distributions at the four spanwise stations are shown in Fig. 25 for a mean angle of attack of 4 deg and a Mach number of 0.825. The oscillation amplitude and frequency are ±1 deg and 10 Hz (k = 0.15), respectively. The pressure peaks vary significantly across the wing span. By comparison with the steady data (Fig. 24), it is observed that the pressure peaks are located near the same chordwise positions as the upper surface mean shocks. The unsteady shock strength decreases nearer the tip region. The phase results in Fig. 25 show that the pressure is generally lagging the wing pitch motion (negative phase) forward of the pitch axis (0.46 fractional chord) and leading the pitch motion aft of the pitch axis. For the two inboard stations where the shocks are located aft of the pitch axis, the lag-to-lead phase shift occurs aft of the upper surface mean shock position.

Mach Number Effects.- Pressure distributions at the inboard station (η = 0.31) are shown in Fig. 26 for seven Mach numbers ranging from 0.4 to 0.85. The wing mean angle of attack is 2 deg. The oscillation amplitude and frequency are 1 deg and 10 Hz, respectively (k ranges from 0.31 at 0.4 Mach number to 0.15 at 0.85 Mach number). The pressure peak is located at the leading edge for the low subsonic Mach numbers but rapidly moves aft as the Mach number increases. At a Mach number of 0.85 the estimated shock location is near the three-quarter chord. For the most part, the phase data show that the pressures lag the motion ahead of the shock and lead behind the shock.

Oscillation Frequency Effects.- Pressure distributions at the inboard chord (0.31 fractional span) are shown in Fig. 27 for seven oscillation frequencies ranging from 2 to 20 Hz (k = 0.03 to 0.31) and an oscillation amplitude of 1 deg. The Mach number and mean angle of attack are 0.8 and 2 deg, respectively. The results show that the frequency effect is large for both the magnitude and phase. As the frequency of oscillation increases, the magnitude of the pressure generally decreases forward of the pitch axis and increases behind the axis. The shock at approximately the 0.35 fractional

chord coincides with the steady-state shock location and appears to decrease in strength as the frequency increases. The phase results show that the pressures lag the motion ahead of the shock and lead the motion behind the shock. The phase angle generally decreases (pressure lags the motion) as the frequency increases. This effect is more pronounced aft of the pitch axis.

Comparison of Measured and Calculated Results

Unsteady pressure calculations were made with two theoretical programs, and the results are compared with measured data. One program is XTRAN3S, (Refs. 19 and 20), a three-dimensional nonlinear transonic code using finite difference methods to approximate a time-accurate solution from the small disturbance potential equation. The version of the code used does not include the effects of viscosity. In order to improve accuracy and agreement with measured data, the XTRAN3S results made use of 1) a revised grid arrangement,[21,22] and 2) small-disturbance equation coefficients derived by the National Aerospace Laboratory of the Netherlands.[23] The other program used for the unsteady pressure comparisons is RHOIV[24], a linear subsonic lifting surface kernel function theory based on the acceleration potential. In addition to the unsteady comparisons, steady pressure comparisons are made using the XTRAN3S program.

Comparisons are made for calculated and measured results at a Mach number of 0.7. The mean angle of attack is 2 deg. The oscillating amplitude and frequency range for the unsteady data are 1 deg and 5 to 20 Hz (k = 0.09 to 0.36), respectively. Rigid pitch motions were used in the unsteady calculations. For XTRAN3S results, the measured wing coordinates were used.

Steady Results

Comparisons of steady upper- and lower-surface pressure distributions at the four span stations are shown in Fig. 28. The comparisons are good over most of the wing. At all spanwise stations the XTRAN3S program accurately predicted both the upper-surface pressures aft of the shock and the lower-surface pressures in the midchord region. The calculated results deviate somewhat from the measurements in the leading-edge region and on the lower surface near the trailing edge. The comparisons in these regions may possibly be improved by including viscous effects in the code and by decreasing the grid spacing for the calculations in this region to account for the bluntness of this airfoil (see Fig. 22). A finer grid may improve the upper-surface pressure-peak definition near the leading edge.

Unsteady Results

Spanwise Pressure Comparison.- Unsteady lifting pressure distributions at two spanwise stations are shown in Figure 29. The comparison includes both measured data and results from XTRAN3S and RHOIV. The XTRAN3S program predicted fairly well the pressure magnitudes at all spanwise stations in the region aft of the shock (located near the leading edge). In the region of the shock the calculations overestimated the leading-edge pressures at the inboard station and under-estimated those pressures at the outboard station. The phase agreement is good over the forward half of the chord at the outboard station. The phase calculations at the inboard station are affected by the overestimated leading-edge shock and are not in good agreement with measured values. The phase agreement also is not good near the trailing edge at both stations. The RHOIV results of the pressure-magnitude show fairly good agreement over the aft two-thirds of the chord. However, at both span stations the magnitude is underestimated in the forward half of the wing and overestimated in the aft portion of the wing. The leading-edge shock, of course, is not predicted by the linear theory. The phase agreement is good over the forward two-thirds of the wing and, in most cases, is better than the XTRAN3S agreement. As with the XTRAN3S results, the phase agreement near the trailing edge is not good.

Concluding Remarks For the Third Model

Both steady and unsteady aerodynamic data were measured on a rectangular wing with a 12% thick supercritical airfoil. The wing was oscillated in pitch to acquire the unsteady data. The purpose of the test was to provide experimental data to assist in the development and assessment of transonic analytical codes. The effect of the wing tip (that is, three-dimensional effects) on the pressure distributions is large. Specifically, the shock location at the outboard sections is considerably farther forward than for inboard sections. Mach number also has a large effect on the shock strength and location. Oscillation frequency has a significant effect on the unsteady pressure magnitudes and phases.

Results from the XTRAN3S nonlinear transonic programs and from the linear RHOIV kernel function program were compared to the measured data. The XTRAN3S steady and unsteady results agreed fairly well with measured data at a Mach number of 0.7. It is believed that the inclusion of viscosity in the analysis and use of a finer grid will give better results, particularly at the wing leading edge. The RHOIV unsteady results were in fair agreement, but, of course, the location or strength of the shock was not predicted.

FOURTH MODEL - HIGH ASPECT RATIO PLANFORM (ELASTIC)

Wind Tunnel Model

General

A delay in the NASA program, Drones for Aerodynamic and Structural Testing (DAST)[25], made the second Aeroelastic Research Wing, ARW-2, available for this wind-tunnel test. The elastic semispan wing used in the present study is the DAST ARW-2 right wing panel. A half-body fuselage was used to simulate the drone fuselage. The center section of the fuselage was similar to the actual drone fuselage in both

diameter and wing location to generate the proper airflow over the inboard area of the wing. Both the fuselage and the wing were mounted on a remotely controlled turntable mechanism located on the tunnel sidewall. Figure 30 shows the wing and fuselage configuration mounted in the wind tunnel.

Geometry

The wing planform and instrumentation locations are shown in Figure 31. The wing has an aspect ratio of 10.3 with a leading-edge sweep angle of 28.8°. The wing was equipped with three hydraulically driven trailing edge control surfaces, two inboard and one outboard. The inboard surfaces were held fixed at 0° deflection and only the outboard surface was deflected statically and dynamically. The outboard surface hinge line was located at 77 percent of local chord.

The wing contour was formed from three different supercritical airfoils. These three airfoils were located at the following spanwise wing stations: the wing-fuselage junction (η = 0.071), the wing planform break (η = 0.426) and the wing tip (η = 1.000) and had thickness-to-chord ratios of 0.15, 0.12 and 0.11, respectively. The three supercritical airfoil shapes and wing twist were defined by the design cruise condition and are described in ref. 26. Straight line interpolation along constant percent chords was used to define the wing contour between these three airfoil sections. The wing construction jig shape was derived from the defined cruise shape, the corresponding loading conditions and the flexibility of the wing structure.

Instrumentation

The locations of the wing instrumentation are shown in Figure 31. The instrumentation consisted of 191 pressure transducers and 10 accelerometers. In addition, strain gauges were located near the wing root to measure bending moments. Differential pressure gauges were mounted in each supply line to the hydraulic actuators of each control surface to measure hinge moments. Small potentiometers were used to measure the control surface angular displacement. The model angle of attack was measured by a servo accelerometer that was mounted near the wing root. Both steady and unsteady pressures were measured using differential pressure transducers referenced to the freestream static pressure. Streamwise rows of upper and lower surface pressure orifices were located at six span stations. The orifice rows were located at η = 0.274, 0.476, 0.599, 0.707, 0.871 and 0.972. The fifth row at η = 0.871 lies along the mid-span of the outboard control surface. All of these surface orifices were connected to pressure transducers by matched tubes having an inner diameter of 0.508mm and a length of 0.457m. To determine the tube transfer functions needed to correct the unsteady pressure data from these matched-tube transducers, simultaneous measurements were also obtained from a row of in situ transducers mounted on the wing upper surface parallel to the fifth row of surface orifices. Dynamic wing deflections were determined using the 10 accelerometers.

Data Acquisition and Analysis

Data from the model instrumentation were acquired using the TDT real-time data acquisition system.[6] The pressure data were acquired using the electronically scanned pressure (ESP) system.[27] The ESP system is a sequential, digital pressure sampling system equivalent to a mechanical scani-valve. All data were digitized in real-time at 250 samples per second and written on magnetic tape for later analysis. Static pressures were measured by all 191 pressure transducers. Each pressure signal was averaged for 1.2 seconds to acquire its mean value.

Dynamic pressure time histories for the three outboard rows of surface orifices and accelerometer time histories were recorded for a minimum of 50 cycles of control surface oscillation. Discrete Fourier transforms of these time histories then provided the magnitude and phase angle at the frequency of the oscillating control surface for each transducer and accelerometer. All phase angles are relative to the position of the oscillating control surface.

Test Results and Discussion

Steady and unsteady pressures were measured for a large number of test conditions in the TDT using Freon as a test medium. The test conditions at which pressure data were taken are shown in Figure 32. Data were taken at Mach numbers of 0.6, 0.7, 0.8, 0.85 and 0.88 and at dynamic pressures of 4.79, 9.58 and 14.37 kPa. At each tunnel condition static pressure data were taken for wing angles of attack of -2 to 4 degrees for the control surface undeflected (δ_0 = 0°). Some of the high angle of attack values were eliminated at the higher dynamic pressures due to maximum bending moment restrictions imposed on the wing. For wing angles of attack of 0 and 2 degrees the control surface static deflection, δ_0, was varied from -8 to 8 degrees. Unsteady pressure data was taken at wing angles of attack of 0 and 2 degrees for control surface oscillation amplitudes of δ equal to 1, 2 and 3 degrees and frequencies of 5, 15 and 20 Hz.

Steady Pressure Results

Span Effects.- Figure 33 shows the steady chordwise pressure distribution at the six span stations for test conditions of (M = 0.8, α = 2°, q = 4.79 kPa and δ_0 = 0°) which are near the design cruise condition. The data show that a shock is present on the upper surface of the wing and the shock chordwise location varies along the span. The steady shock location, in terms of local chord, moves aft between 27 and 87 percent span then moves forward between 87 and 97 percent span.

Mach Number Effects.- Figure 34 shows the steady pressure distributions at the 87 percent span station for five Mach numbers for 2° angle of attack; a dynamic pressure of 4.79 kPa and an outboard mean control surface deflection, δ_0, of 0°. As Mach number increases, a shock can be seen to have formed near 30 percent chord at a Mach number equal of 0.80 and to move aft to about 70 percent chord at a Mach number equal to

0.88. Attached flow is indicated at all Mach numbers except at a Mach number of 0.88 where the pressure distribution indicates that there is flow separation on the upper surface near the trailing edge.

Angle of Attack Effects.- The variation of the steady lifting pressure with angle of attack at Mach number of 0.80 and dynamic pressure of 4.79 kPa is shown in Figure 35 for the 87 percent span station. The shock develops and moves aft as the angle of attack increases from -2 to 4 degrees.

Unsteady Pressure Results

Mach Number Effects.- Figure 36 shows the variation of the unsteady lifting pressure distribution with Mach number at the 87 percent span station. The outboard control surface was oscillated with an amplitude $\delta = 1°$ about a mean deflection of $\delta_0 = 0°$ at 15 Hz. The magnitude and phase components of the unsteady lifting pressure are plotted versus percent chord. For all Mach numbers a peak in the pressure magnitude occurs just forward of the control surface hinge line location. An additional peak in the magnitude can be seen to occur at the mean shock location for Mach numbers 0.70 to 0.85 (see Figure 33). This peak probably is caused by the shock motion generated by the oscillatory control surface motion. The mean shock location can be seen to move aft with increasing Mach number. The mean shock peak and control hinge line peak appear to merge at a Mach number of 0.85. The peak in the pressure magnitude near the control surface hinge line increases with increasing Mach number through a Mach number of 0.85, but then drops to the lowest value at a Mach number of 0.88. In addition, no mean shock peak can be seen in the pressure magnitude at a Mach number of 0.88. These phenomena may be attributable either to the flow separation which occurs in the trailing edge region of the wing at a Mach number of 0.88, or to the transducers being too far apart near the hinge line to show the existance of a peak.

Frequency Effects.- Figure 37 shows the variation of the unsteady lifting pressure with oscillation frequency at the 87 percent span station. At the upper surface mean shock location the magnitude of the unsteady pressure increases with increasing frequency from 5 to 20 Hz except at 10 Hz. The magnitude peak for the 10 Hz oscillation is much greater than that for the other frequencies, probably because this 10 Hz frequency was very close to the wing first bending frequency of 8.3 Hz (wind-off).

Wing Deflections

For rigid wing pressure studies, the assumption is made that the wing does not deform, and therefore only the measured pressure distributions are needed. In contrast, for elastic wing pressure studies, the above assumption is not true. Therefore both the measured pressure distributions and the corresponding measured deformed wing shape are needed to define the aerodynamic loading characteristics for a given wing configuration.

In the present study a technique known as stereophotogrammetry was used to measure the static wing deflections.[28] The stereophotogrammetry deflection results are not available at this time. However, during these tests some deflection measurements of the wing tip were made using a cathetometer instrument focused on a straight line drawn on the tip of the wing. Both vertical deflections and angular deflections of the wing tip were measured at selected test points. Results of these wing tip deflection measurements at a Mach number of 0.80 and an angle of attack of 0° are shown in Figure 38. The variation of the wing tip vertical deflection with dynamic pressure is presented at the top of Figure 38 and the associated wing tip twist angle is presented at the bottom of Figure 38. Clearly, the elastic wing exhibits significant nonlinear tip deflections, with vertical deflections of over 100 mm and a negative tip twist of over 3 degrees occurring at the higher dynamic pressures.

The present study used selectively spaced accelerometers mounted on the wing to obtain dynamic wing deflections for all wing tests of forced oscillatory motion. A discrete Fourier analysis was performed on each accelerometer signal at the known frequency of oscillation to obtain the amplitude of acceleration which was then integrated twice to obtain magnitude of the motion at the corresponding wing location.

Figure 39 shows the wing deflection mode shape derived from the accelerometer data for the cases shown in Figure 36. The vertical deflection at the elastic axis is plotted for four oscillation frequencies. The elastic axis is located midway between the accelerometers shown in Figure 31. As mentioned, at excitation frequencies near 10 Hz the coupling of the forcing function frequency with the wing's first bending mode caused large dynamic wing deflections. Testing at 10 Hz was therefore discontinued after tests at only a few wing and tunnel conditions.

Concluding Remarks For the Fourth Model

Steady and unsteady pressures were measured on an elastic high-aspect-ratio supercritical wing. Static and dynamic wing deflections were also measured. An outboard trailing-edge control surface was oscillated at various amplitudes and frequencies to obtain unsteady data. Test conditions covered a wide range of Mach number from 0.60 to 0.90, dynamic pressure from less than 2.39 to over 14.37 kPa. Model parameters variations included wing angle of attack from -2 to 4 degrees, control surface mean deflection angle from -8 to 8 degrees and control surface oscillation amplitudes of 1, 2, and 3 degrees at frequencies of 5, 10, 15, and 20 Hz. Briefly, the steady pressure distributions show that span location, Mach number and angle of attack have a large effect on the mean shock strength and chordwise location. The unsteady pressure distributions show that large peaks in the pressure magnitude occur due to both the oscillatory control surface and to the motion of the mean shock location. Frequency effects were shown to be non-linear and exceedingly large if the oscillatory frequency occurs near a natural mode of the wing structure. Static tip deflec-

tions were shown to be large (100 mm of vertical deflection and 3 degrees of twist) and nonlinear with increasing dynamic pressure.

Summary

Transonic unsteady pressure measurements at the NASA Langley Research Center over the past decade have been described. Four models which were tested in the TDT have been described along with their construction and data gathering procedures. For each model, some selected results have been presented, which are representative of the data base being built.

Though not included in this paper an unsteady pressure study was completed recently in the Langley 0.3m Transonic Cryogenic Tunnel. These tests of a 14 percent thick supercritical airfoil were conducted to develop and test experimental techniques for measuring unsteady pressures in a cryogenic environment at Reynolds number up to 35 million.

As NASA Langley Research Center enters the second decade of unsteady pressure measurements, active studies presently include the following: 1) tests of a novel 2-D airfoil flutter model mount system which will allow unsteady pressure measurement on airfoils at subcritical and critical flutter conditions, 2) tests of a canard-wing configuration, and 3) follow-on test of the DAST ARW-2 elastic wing.

References

[1]Edwards, J. W.; Bland, S. R.; and Seidel, D. A.: "Experience with Transonic Unsteady Aerodynamic Calculations," NASA TM 86278, August 1984.

[2]Hess, R. W.; Wynne, E. C.; and Cazier, F. W., Jr.: Static and Unsteady Pressure Measurements on a 50 Degree Clipped Delta Wing at M = 0.9. NASA TM 83297, April 1982.

[3]Sandford, M. C.; Ricketts, R. H.; Cazier, F. W., Jr.; and Cunningham, H. J.: Transonic Unsteady Airloads on an Energy Efficient Transport Wing With Oscillating Control Surfaces. Journal of Aircraft, Vol. 18, No. 7, July 1981, pp. 557-561.

[4]Ricketts, R. H.; Sandford, M. C.; Seidel, D. A.; and Watson, J. J.: Transonic Pressure Distributions on a Rectangular Supercritical Wing Oscillating in Pitch. Journal of Aircraft, Vol. 21, No. 8, August 1984, pp. 567-582.

[5]Seidel, D. A.; Sandford, M. C.; and Eckstrom, C. V.: "Measured Unsteady Transonic Aerodynamic Characteristics of an Elastic Supercritical Wing With an Oscillating Control Surface," to be presented at the AIAA/ASME/ASCE/AHS 26th Structures, Structural Dynamics and Materials Conference, Orlando, Florida, April 15-17, 1985, AIAA Paper No. 85-0598-CP.

[6]Cole, P. H.: Wing Tunnel Real-Time Data Acquisition System, NASA TM-80081, April 1979.

[7]Mason, W. H.; Ballhaus, W. F.; Mackenzie, C.; Frick, J.; and Stern, M.: An Automated Procedure for Computing the Three-Dimensional Transonic Flow Over Wing-Body Combinations, Including Viscous Effects. AFFDL-TR-77-122.

[8]Watson, Judith J.: "Elastic Deformation Effects on Aerodynamic Characteristics for a High-Aspect-Ratio Supercritical-Wing Model," NASA TM 83286, May 1982.

[9]Bergmann, G. E.; and Sevart, F. D.: "Design and Evaluation of Miniature Control Surface Actuation Systems for Aeroelastic Models," Journal of Aircraft, Vol. 12, March 1975, pp. 129-134.

[10]Sandford, Maynard C.; Ricketts, Rodney H.; and Cazier, F. W., Jr.: "Transonic Steady- and Unsteady-Pressure Measurements on a High-Aspect-Ratio Supercritical-Wing Model With Oscillating Control Surfaces," NASA TM-81888, 1980.

[11]Sandford, Maynard C.; Ricketts, Rodney H.; Watson, Judith J.: "Subsonic and Transonic Pressure Measurements on a High-Aspect-Ratio Supercritical-Wing Model With Oscillating Control Surfaces," NASA TM-83201, 1981.

[12]Sandford, Maynard C.; Ricketts, Rodney H.: Steady-and Unsteady-Pressure Measurements on a Supercritical-Wing Model With Oscillating Control Surfaces at Subsonic And Transonic Speeds," NASA TM-84543, 1983.

[13]Many Authors: "Supercritical Wing Technology - A Progress Report on Flight Evaluations," NASA SP-301, 1972.

[14]Rowe, W. S.; Sebastian, J. D.; and Petrarca, J. R.: "Reduction of Computer Usage Costs in Predicting Unsteady Aerodynamic Loadings Caused by Control Surface Motions--Analysis and Results," NASA CR-3009, March 1979.

[15]McCain, William E.: "Comparison of Measured and Calculated Airloads on an Energy Efficient Transport Wing Model Equipped With Oscillating Control Surfaces," AIAA Paper No. 84-0301, January 1984.

[16]Ricketts, R. H.; Watson, J. J.; Sandford, M. C.; and Seidel, D. A.: "Geometric and Structural Properties of a Rectangular Supercritical Wing Oscillated in Pitch for Measurement of Unsteady Transonic Pressure Distributions," NASA TM-85673, Nov. 1983.

[17]Tijdeman, H.: "Investigations of the Transonic Flow Around Oscillating Airfoils," National Aerospace Laboratory, Amsterdam, NLRTR-77090U, 1977 (available from DTIC as ADB027633).

[18]Ricketts, R. H.; Sandford, M. C.; Watson, J. J., and Seidel, D. A.: "Subsonic and Transonic Unsteady- and Steady-Pressure Measurements on a Rectangular Supercritical Wing Oscillated in Pitch," NASA TM-85765, July 1984.

[19]Borland, C. J.; and Rizzetta, D. P.: "Nonlinear Transonic Flutter Analysis," AIAA Paper 81-0608, April 1981.

[20]Borland, C. J.; and Rizzetta, D. P.: "Nonlinear Transonic Flutter Analysis," AIAA Journal, Vol. 20, No. 11, pp. 1605-1615, November 1985.

[21]Seidel, D. A.; Bennett, R. M.; and Whitlow, W., Jr.: "An Exploratory Study of Finite Difference Grids for Transonic Unsteady Aerodynamics," AIAA Paper 83-0503 (also available as NASA TM-84583, Dec. 1982).

[22]Seidel, D. A.; Bennett, R. M.; and Ricketts, R. H.: "Some Recent Applications of XTRAN3S," AIAA Paper 83-1811 (also available as NASA TM-85641, May 1983).

[23]Van der Vooren, J.; Sloof, J. W.; Hizing, G. H.; and Van Essen, A.: "Remarks on the Suitability of Various Transonic Perturbation Equations to Describe Three-Dimensional Transonic Flow - Examples of Computations Using a Fully-Conservative Rotated Difference Scheme," Proceedings of Symposium Transonicum II, Springer-Verlag, Berlin, 1976, pp. 557-566.

[24]Redman, M. C.; and Rowe, W. S.: "Prediction of Unsteady Aerodynamic Loadings Caused by Leading Edge and Trailing Edge Control Surface Motions in Subsonic Compressible Flow - Computer Program Description," NASA CR-132634, 1975.

[25]Murrow, H. N.; and Eckstrom, C. V.: "Drones for Aerodynamic and Structural Testing (DAST) - A Status Report," Journal of Aircraft, Vol. 16, No. 8, August 1979, pp. 521-526.

[26]Byrdsong, T. A.; and Cuyler, W. B., Jr.: Wind-Tunnel Investigation of Longitudinal and Lateral-Directional Stability and Control Characteristics of a 0.237-Scale Model of a Remotely Piloted Research Vehicle With a Thick, High-Aspect-Ratio Supercritical Wing. NASA TM-81790, July 1980.

[27]Chapin, W. G.: Dynamic-Pressure Measurements Using an Electronically Scanned Pressure Module. NASA TM-84650, July 1983.

[28]Brooks, J. D.; and Beamish, J. K.: Measurement of Model Aeroelastic Deformations in the Wind Tunnel at Transonic Speeds Using Stereophotogrammetry. NASA TP-1010, October 1977.

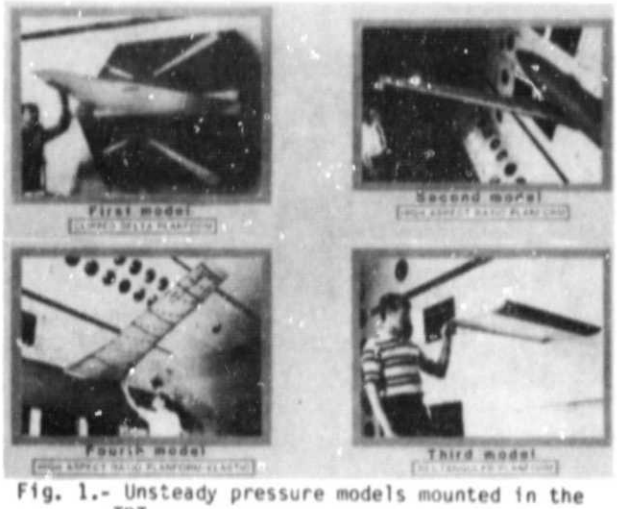

Fig. 1.- Unsteady pressure models mounted in the TDT.

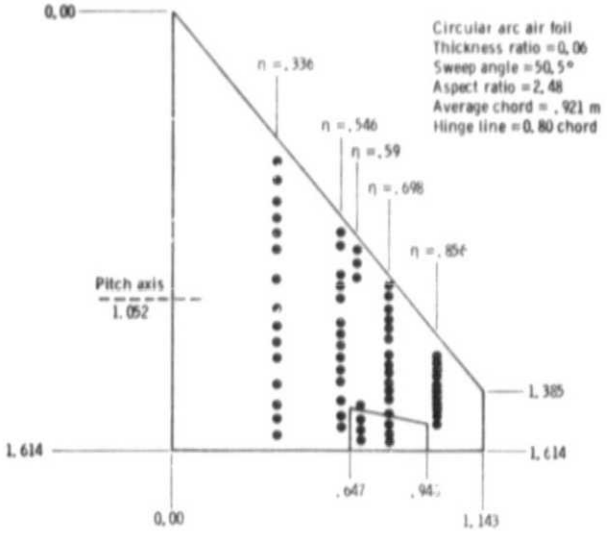

Fig. 2.- Sketch of the first model.

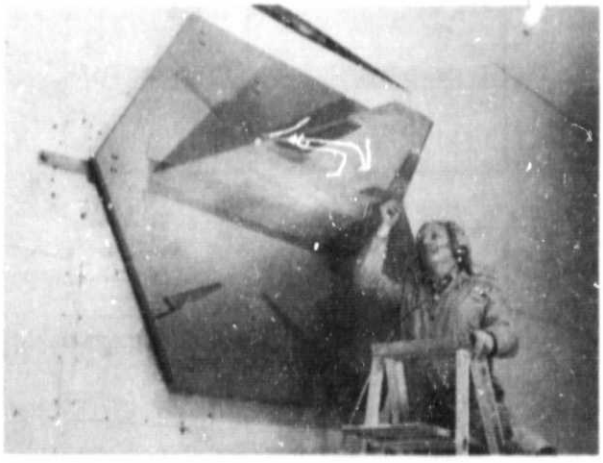

Fig. 3.- Photograph of the first model, clipped delta wing and splitter plate, mounted in TDT.

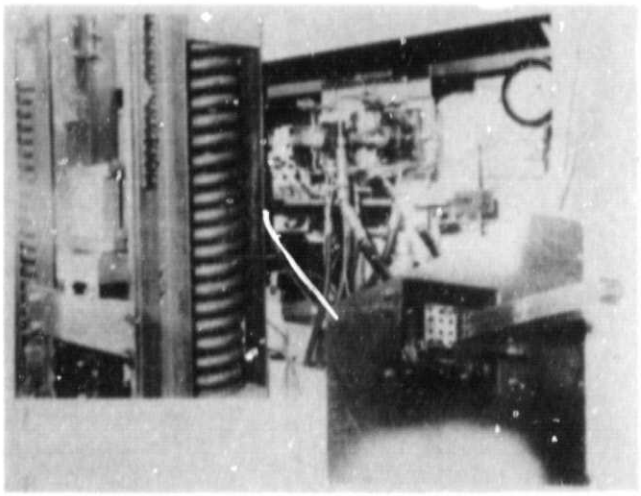

Fig. 4.- Wing hydraulic drive system and tapered support shaft.

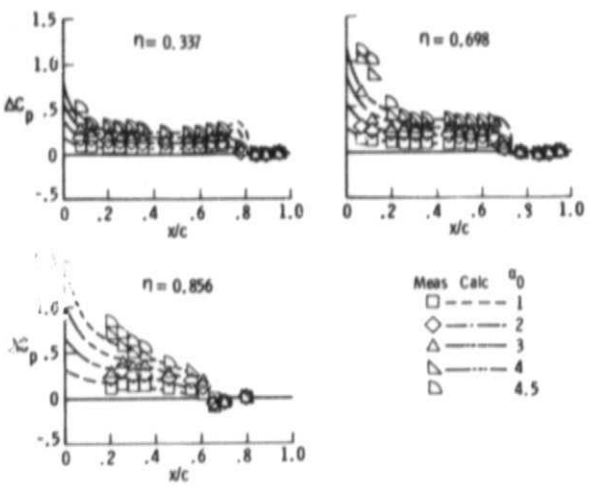

Fig. 5.- Steady lifting pressure distribution variation with angle of attack at M = 0.90 for three span stations.

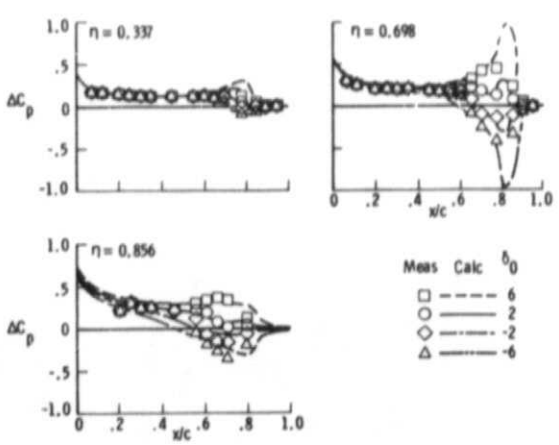

Fig. 6.- Steady lifting pressure distribution variation with control surface deflection at M = 0.90 for three span stations.

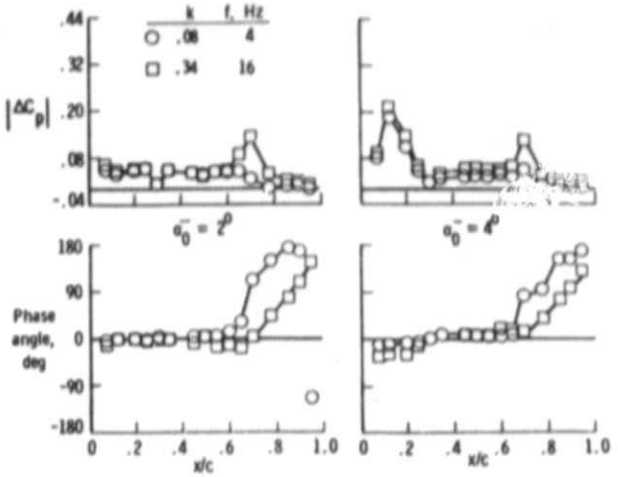

Fig. 7.- Unsteady lifting pressure magnitude and phase angle distribution variation with pitch oscillations of α = 0.5°, M = 0.90 and η = 0.70.

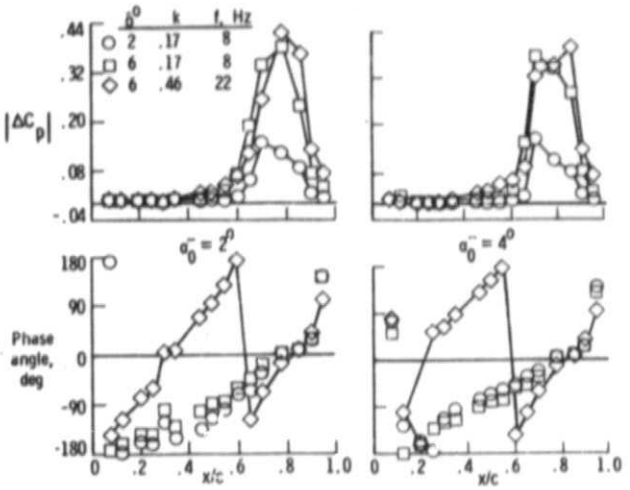

Fig. 8.- Unsteady lifting pressure magnitude and phase angle distribution variation with control surface oscillations at M = 0.90 and η = 0.70.

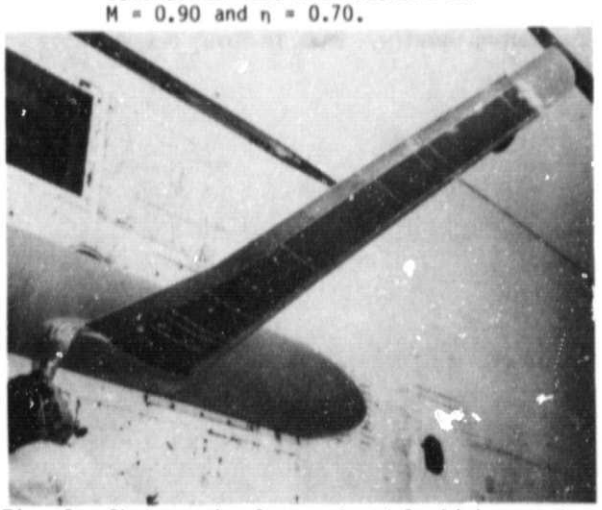

Fig. 9.- Photograph of second model, high-aspect ratio planform mounted in TDT.

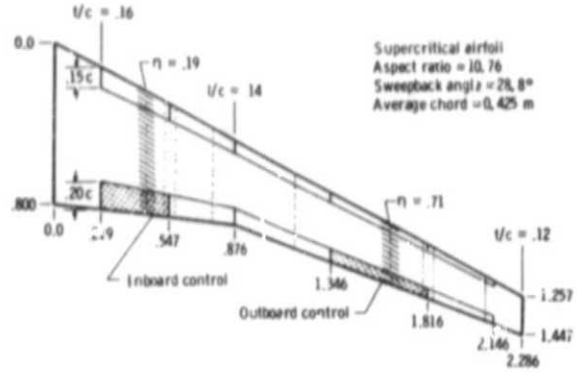

Fig. 10.- Sketch of second model, high-aspect-ratio planform.

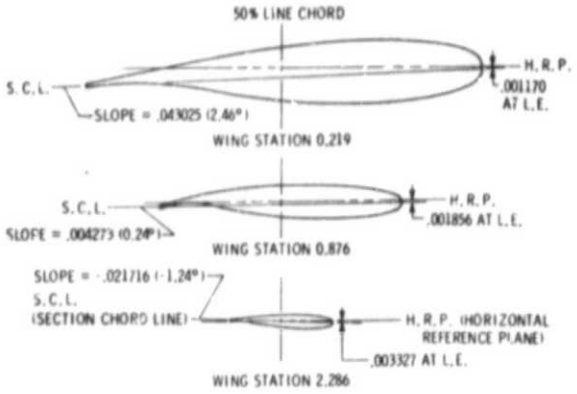

Fig. 11.- Supercritical airfoil shapes at three span stations for the high aspect ratio model.

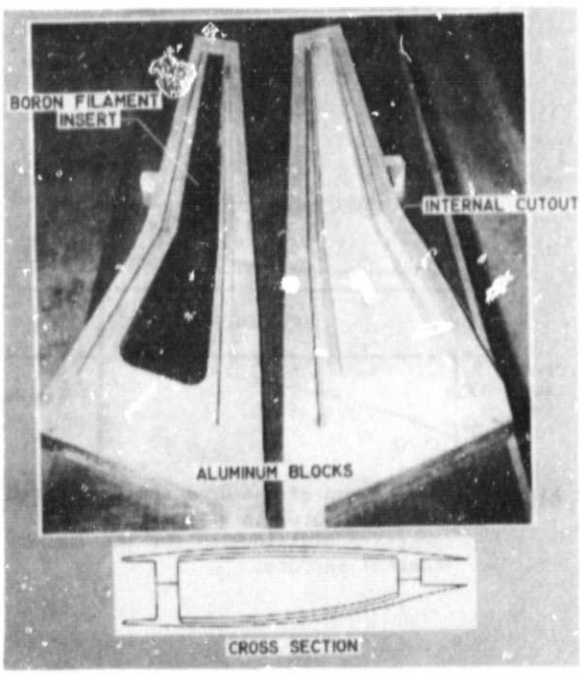

Fig. 12.- Illustratic of wing box construction.

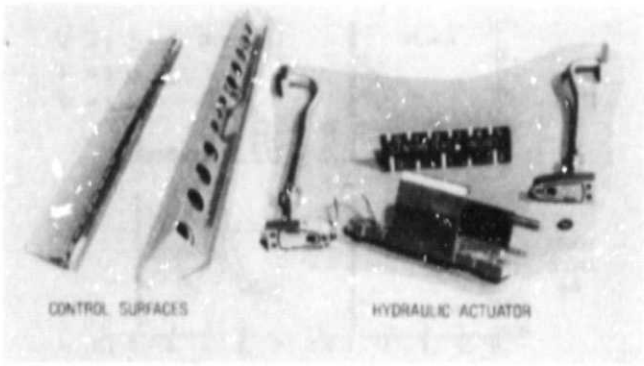

Fig. 13.- Photograph of typical control surface and hydraulic actuator.

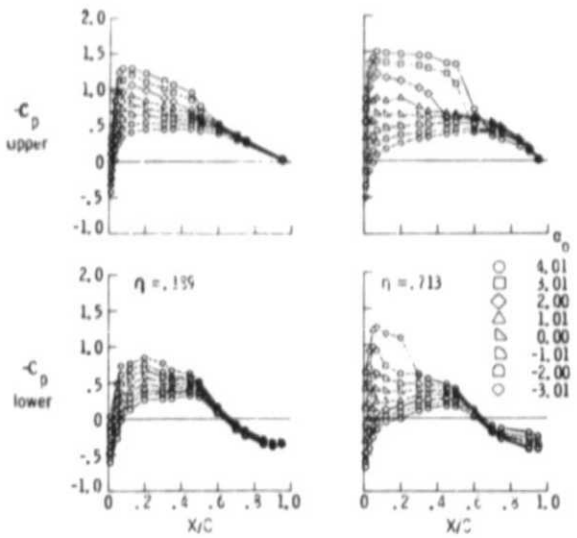

Fig. 14.- Steady pressure distribution variation with angle of attack at M = 0.78 for two span stations.

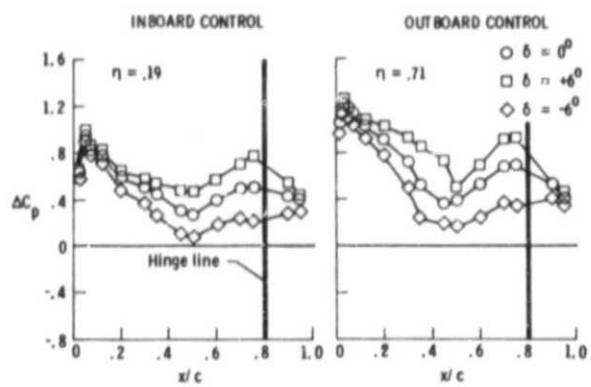

Fig. 15.- Steady lifting pressure distribution variation with inboard and outboard control surface deflection at M = 0.78 and α_0 = 2.05°.

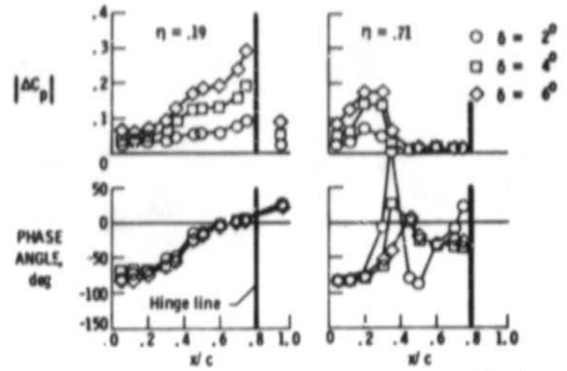

Fig. 16.- Inboard control surface oscillating deflection results.

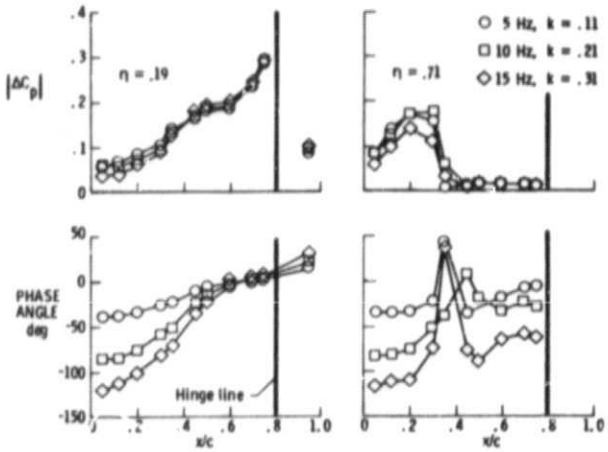

Fig. 17.- Inboard control surface oscillating frequency results.

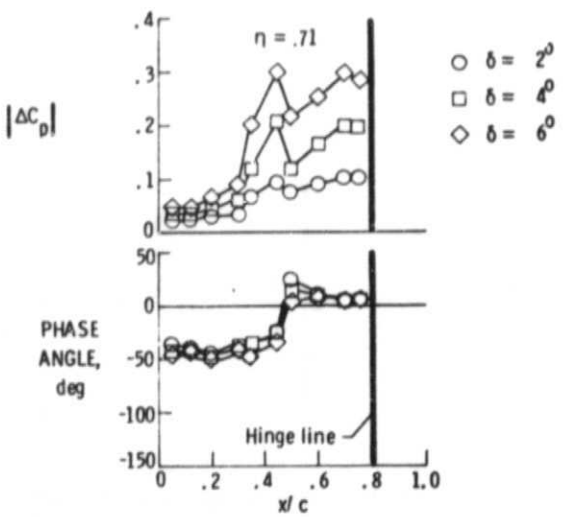

Fig. 18.- Outboard control surface oscillating deflection results.

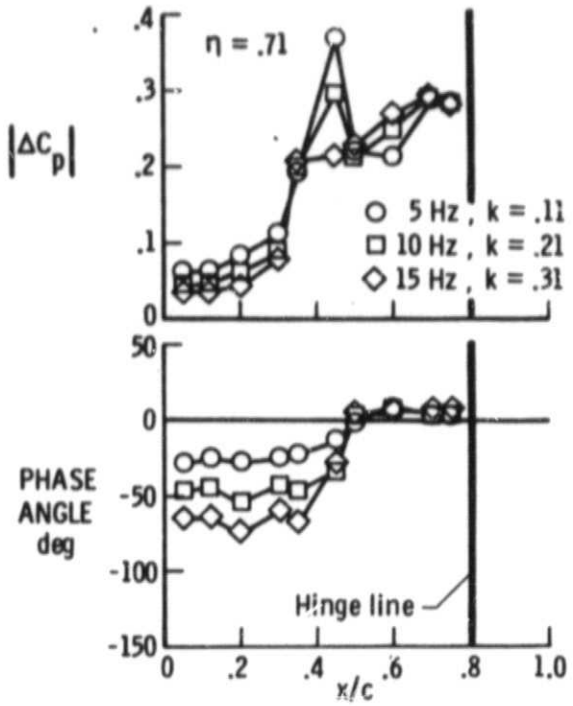

Fig. 19.- Outboard control surface oscillating frequency results.

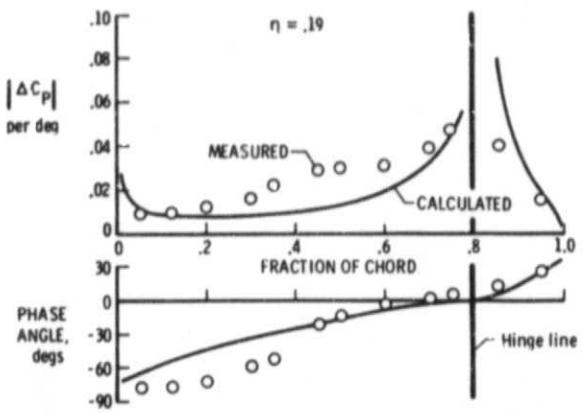

Fig. 20.- Comparison of measured and calculated (RHOIV) chordwise unsteady lifting pressure distribution for the inboard control surface.

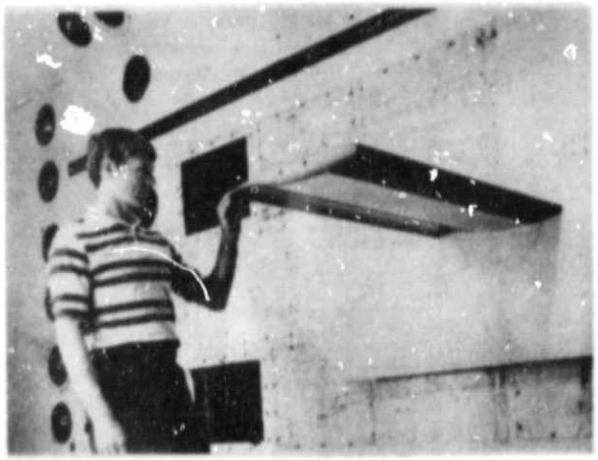

Fig. 21.- Photograph of the third model, rectangular planform mounted in TDT.

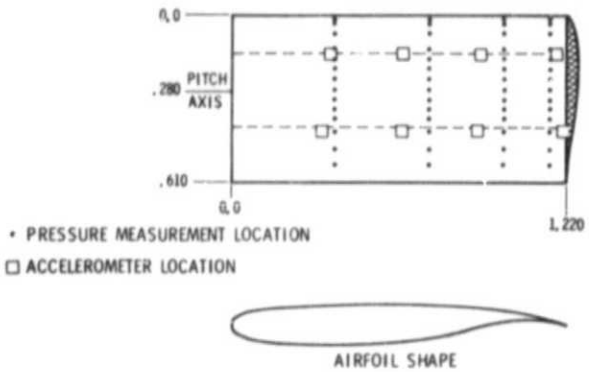

Fig. 22.- Sketch of planform and airfoil shape of third model (dimensions in feet).

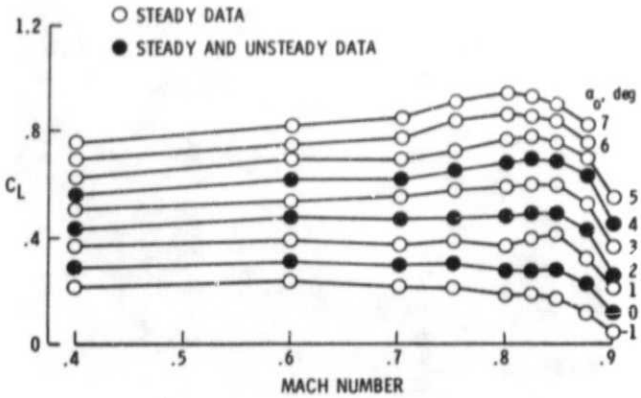

Fig. 23.- Variation of total lift coefficient with Mach number for various angles of attack.

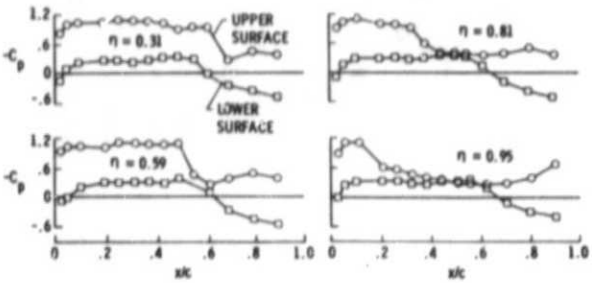

Fig. 24.- Steady pressure distributions at four span stations; M = 0.825, α_o = 4°.

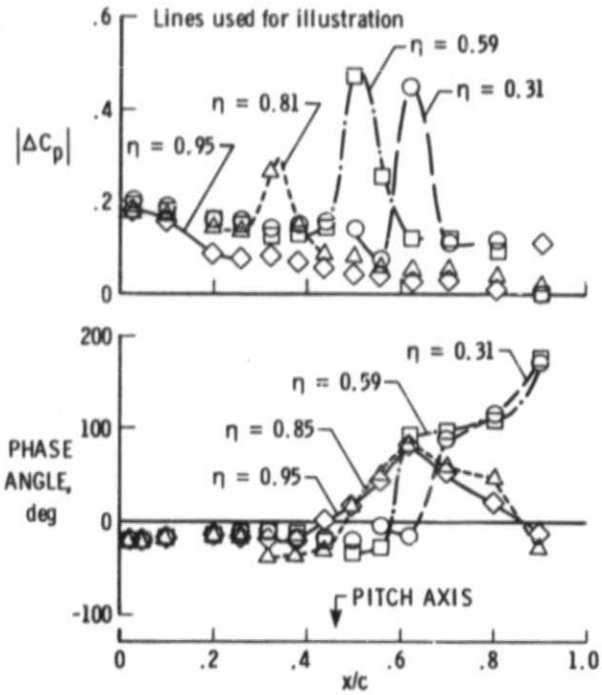

Fig. 25.- Effects of span station on unsteady lifting pressure magnitude and phase distribution; M = 0.825, α_o = 4°, f = 10 Hz, α = 1°.

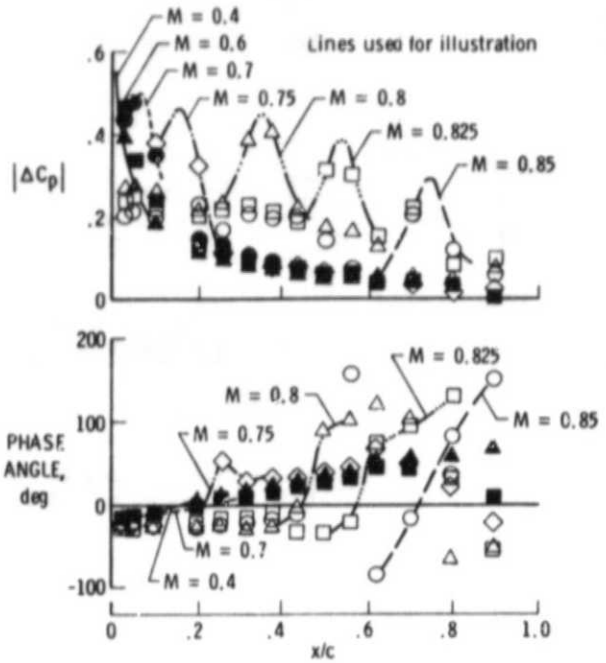

Fig. 26.- Effects of Mach number on unsteady lifting pressure magnitude and phase distribution; η = 0.31, α_0 = 2°, f = 10 Hz, α = 1°.

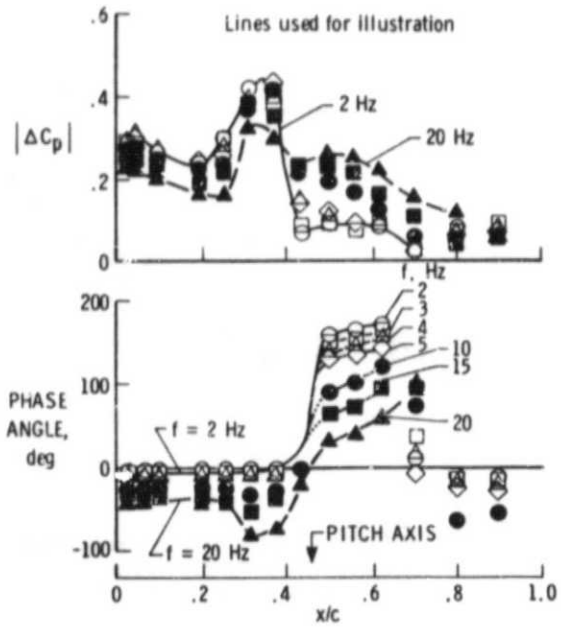

Fig. 27.- Effects of frequency on unsteady lifting pressure magnitude and phase distribution; M = 0.80, η = 0.31, α_0 = 2°, f = 10 Hz, α = 1°.

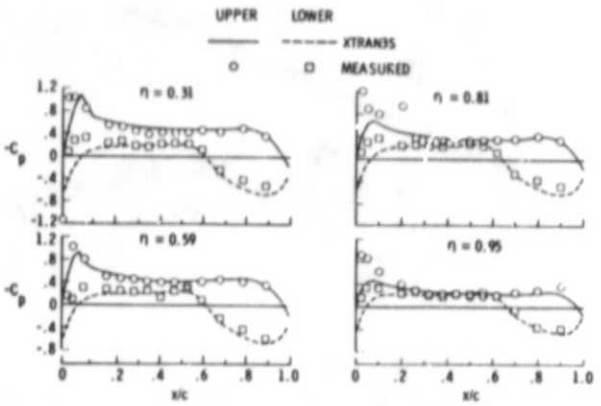

Fig. 28.- Comparison of measured and calculated steady pressure distributions for four span stations; M = 0.7, α_0 = 2°.

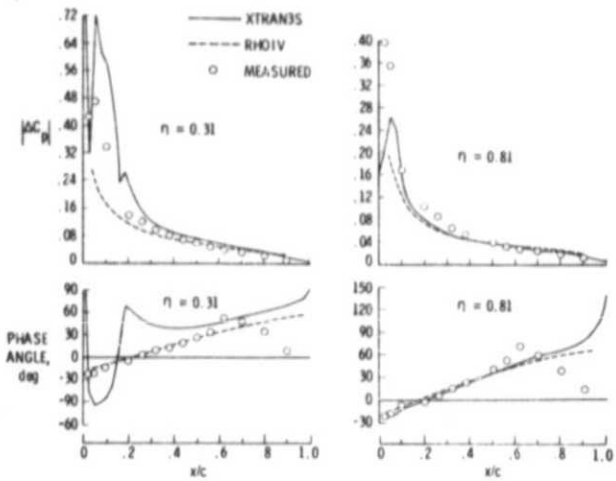

Fig. 29.- Comparison of measured and calculated unsteady pressure magnitude and phase distributions for two span stations; M = 0.7, α_0 = 2°, f = 10 Hz, α = 1°.

Fig. 30.- Photograph of the fourth model high-aspect-ratio planform (elastic) mounted in TDT.

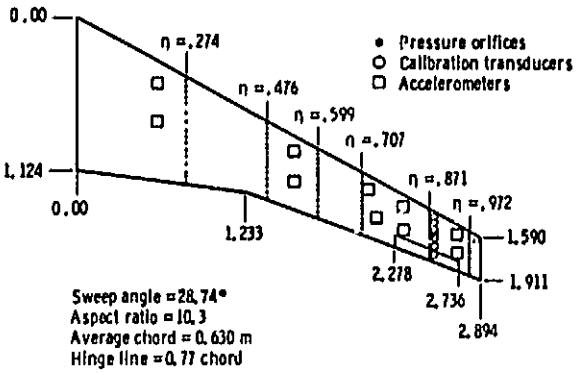

Fig. 31.- Sketch of planform and instrumentation locations for the fourth model.

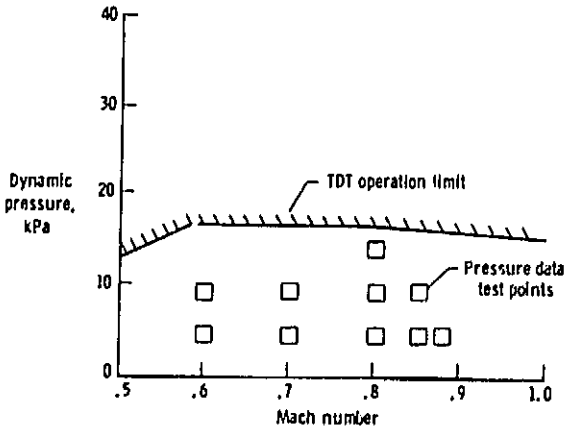

Fig. 32.- TDT test condition for the fourth model, high-aspect-ratio (elastic).

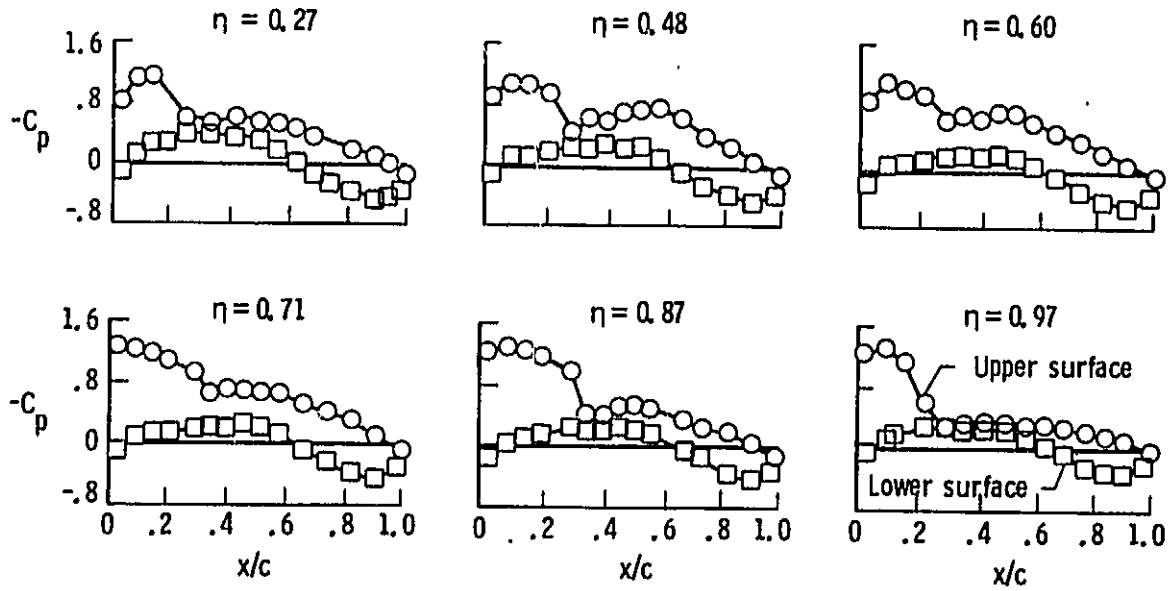

Fig. 33.- Steady pressure distributions for six span stations; M = 0.80, α_0 = 2°, q = 4.79 kPa, δ_0 = 0°.

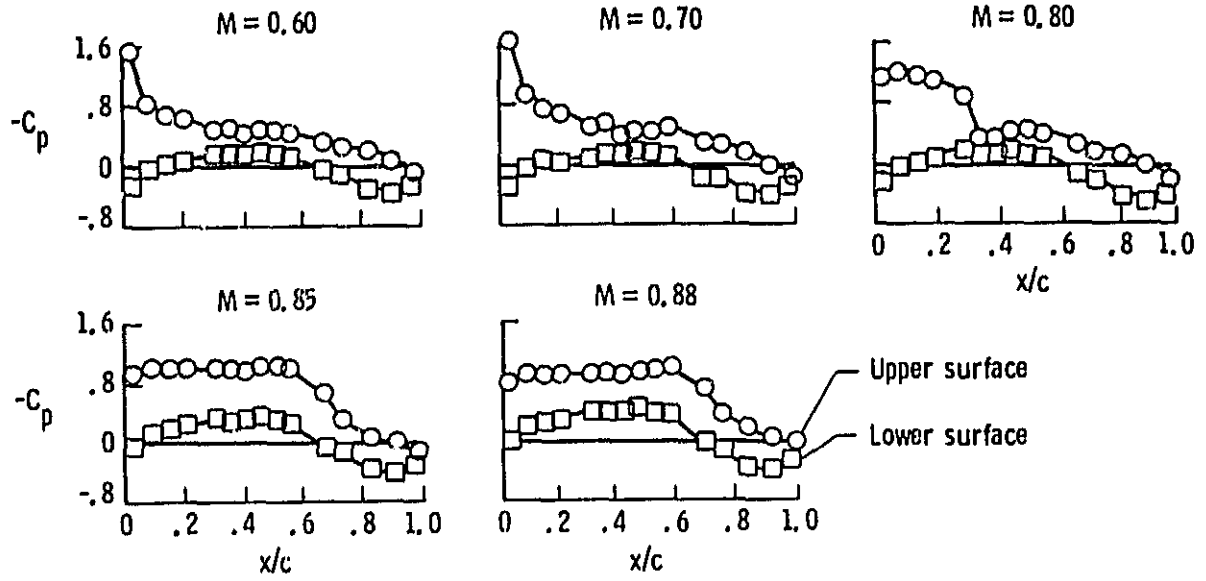

Fig. 34.- Steady pressure distributions for six Mach numbers; $\eta = 0.87$, $\alpha_0 = 2°$, $q = 4.79$ kPa, $\delta_0 = 0°$.

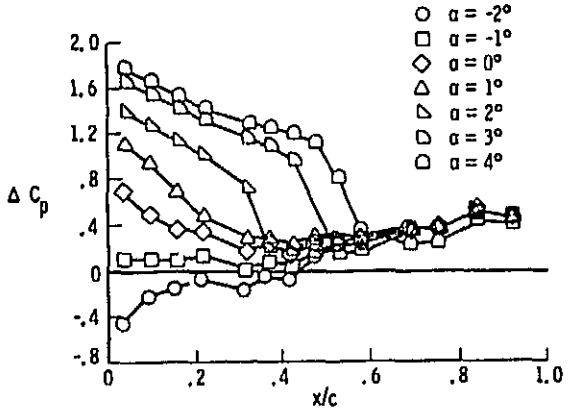

Fig. 35.- Steady lifting pressure distributions for various angles of attack; $M = 0.80$, $\eta = 0.87$, $q = 4.79$ kPa, $\delta_0 = 0°$.

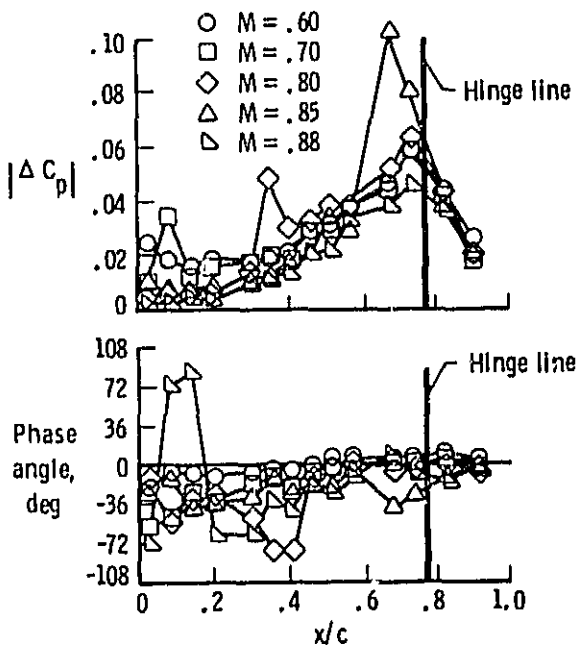

Fig. 36.- Effect of Mach number on unsteady lifting pressure magnitude and phase distribution; $\eta = 0.87$, $\alpha_0 = 2°$, $q = 4.79$ kPa, $\delta_0 = 0°$, $\delta = 1°$, $f = 15$ Hz.

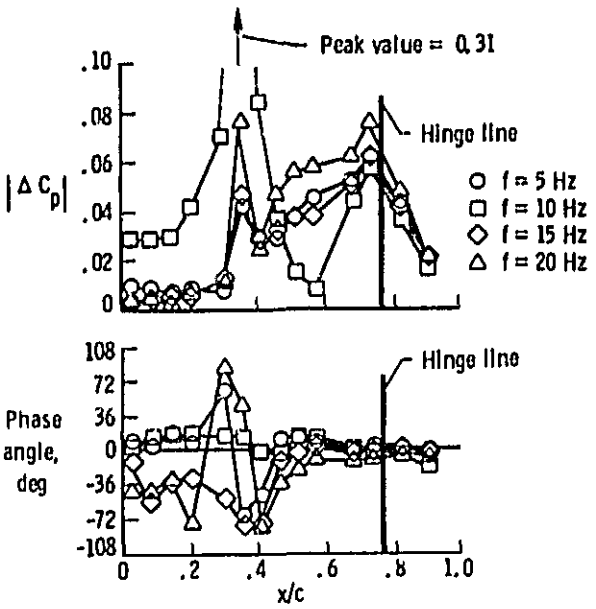

Fig. 37.- Effect of frequency on unsteady lifting pressure magnitude and phase distribution; M = 0.80, α = 2°, q = 4.79 kPa, δ_0 = 0°, δ = 1°, η = 0.87.

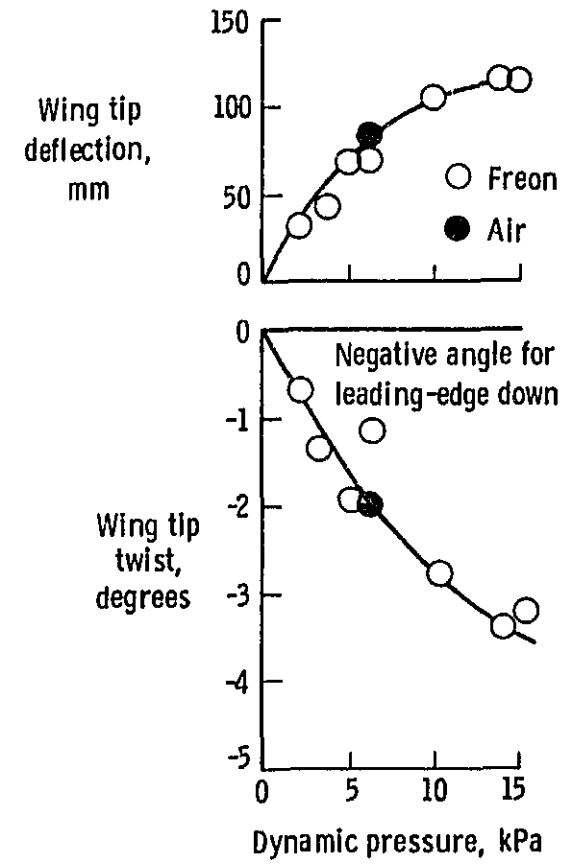

Fig. 38.- Measured wing tip vertical deflection and twist variation with dynamic pressure at M = 0.80 and α_0 = 0°.

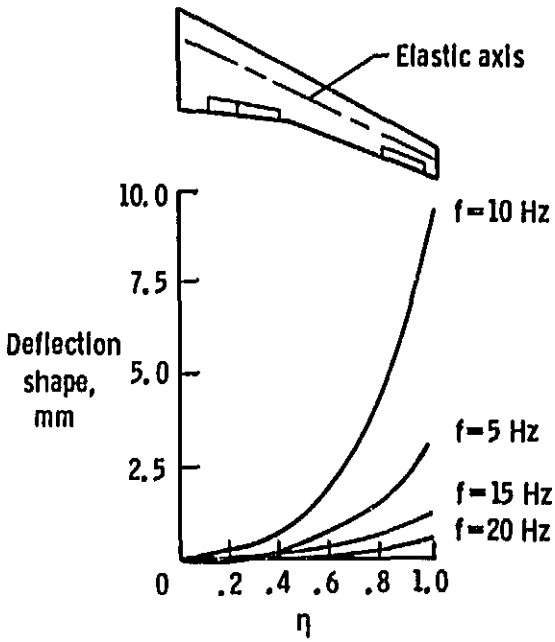

Fig. 39.- Effect of frequency on wing first bending mode shape amplitude at the elastic axis; M = 0.80, α = 2°, q = 4.79 kPa, δ_0 = 0°, δ = 1°.